Available online at www.sciencedirect.com
SCIENCE DIRECT®
Journal of Sound and Vibration 283 (2005) 507–523
JOURNAL OF SOUND AND VIBRATION
www.elsevier.com/locate/jsvi

Prediction of maximum unbalance responses of a gear-coupled two-shaft rotor-bearing system

An Sung Lee[a,*], Jin Woong Ha[b]

[a]*Rotor Dynamics Group, Korea Institute of Machinery and Materials, Yoosung, P.O. Box 101, Daejeon 305-600, Republic of Korea*
[b]*R&D Department, Century Corporation, Asansi, Chungnam 336-842, Republic of Korea*

Received 8 August 2003; received in revised form 3 March 2004; accepted 28 April 2004
Available online 2 November 2004

Abstract

A general method was presented for obtaining the unbalance response orbit of a gear-coupled two-shaft rotor-bearing system, based on the finite element approach. Specifically, analytical solutions of the maximum and minimum radii of the orbit were proposed. The method was applied to the unbalance response analysis of a 600 kW turbo-chiller rotor-bearing system, having a bull-pinion speed increasing gear. Bumps in the unbalance responses were observed at the first torsional natural frequency because of the coupling between the lateral and torsional dynamics due to gear meshing. In addition, the analytical solutions were validated with results obtained by a full numerical approach. The proposed method can be generally applied to an analysis of the unbalance response orbits of dual-shaft rotor-bearing systems coupled by bearings as well, which are often found in aerospace gas turbine engines.

1. Introduction

It is known that for a general rotor system with a shaft diameter to length ratio, $D/L, > 0.01$, the coupled effect of the lateral and torsional vibrations may be neglected [1]. However, for a gear box or geared rotor-bearing system complex couplings between the lateral vibrations, the torsional

*Corresponding author. Tel.: +82-42-868-7356, fax: +82-42-868-7440.
E-mail address: aslee@kimm.re.kr (A.S. Lee).

0022-460X/$ - see front matter © 2004 Elsevier Ltd. All rights reserved.
doi:10.1016/j.jsv.2004.04.037

vibrations and the lateral and torsional vibrations may well arise as the result of gear meshing effects [2]. In some cases these coupled vibrations may lead to design concerns relative to the free vibration and unbalance response characteristics of the systems, compared to those obtained in the absence of the coupling effects. To assure the reliable low-vibration design of high-performance turbomachinery which incorporate a speed increasing or decreasing gear pair, a precise rotordynamic analysis is required, which takes into consideration the coupling mechanism of the gear meshing at a detail design stage.

Concerning free vibration investigations of geared rotor-bearing systems, based on the general finite element modeling considering the translational, rotary and torsional degrees of freedom with the gyroscopic effect, Lee et al. [3] and Rao et al. [4] investigated the coupled lateral–torsional characteristics of a speed-increasing geared turbo-chiller and a speed-reduction geared turbo-generator, respectively.

Concerning unbalance response investigations of geared rotor-bearing systems, based on the finite element modeling, Neriya et al. [5] and Kahraman et al. [6] carried out investigations utilizing the modal analysis technique. Besides, based on the transfer matrix modeling, Iida et al. [7] and Iwatsubo et al. [8] reported on studies utilizing the usual procedure of solving simultaneous equations, and Choi and Mau [9] utilizing the frequency branching technique. Further, concerning unbalance response investigations of dual shaft rotor-bearing systems coupled by bearings, based on the transfer matrix modeling, Hibner [10], Li et al. [11] and Gupta et al. [12] carried out investigations utilizing the usual procedure of solving simultaneous equations. However, all the above investigations resulted in full numerical solutions of the unbalance responses of coupled two-shaft rotor-bearing systems.

On the other hand, Rao [13] suggested analytical closed-form expressions for the major and minor axis radii of the unbalance response orbit for one-shaft rotor-bearing system. Rao et al. [14] and Shiau et al. [15] investigated the lateral responses of geared rotors due to short circuit torsional excitation.

In this paper a general method is presented for obtaining the unbalance response orbit based on the finite element approach of a gear-coupled two-shaft rotor-bearing system, where the shafts rotate at their different respective speeds. Specifically, analytical solutions of the maximum and minimum radii of the orbit are proposed. The method is then applied to the unbalance response analysis of a 600 kW turbo-chiller rotor-bearing system, having a bull-pinion speed increasing gear. In addition, the validity of the proposed analytical solutions of the orbit radii is tested against those obtained fully numerically.

2. Finite element modeling

A displacement vector of a gear pair can be defined from the pressure line coordinate system as shown in Fig. 1 by

$$\{q^{G'}\} = \left\lfloor u_1^{G'} \;\; v_1^{G'} \;\; \theta_{X1}^{G'} \;\; \theta_{Y1}^{G'} \;\; u_2^{G'} \;\; v_2^{G'} \;\; \theta_{X2}^{G'} \;\; \theta_{Y2}^{G'} \;\; \theta_{Z1}^{G'} \;\; \theta_{Z2}^{G'} \right\rfloor^{\mathrm{T}}, \tag{1}$$

where u, v, θ_X and θ_Y are the translational and rotary degrees of freedom and θ_Z the torsional degree of freedom, and the subscripts 1 and 2 indicate the driving and driven gears. From the

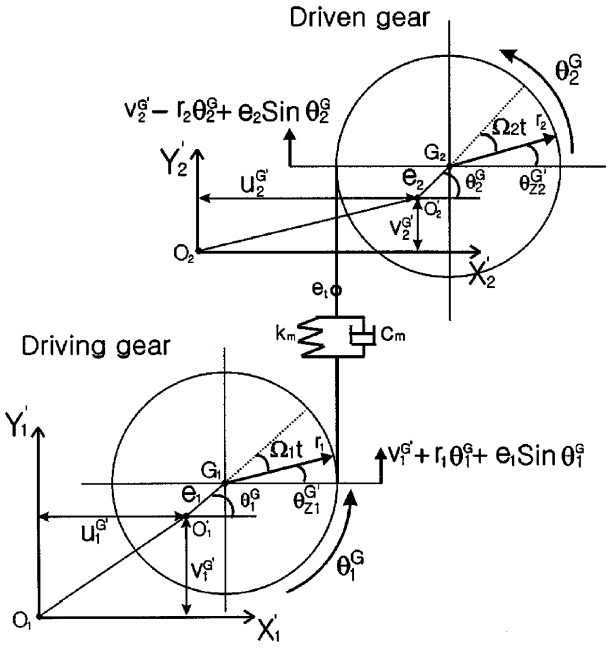

Fig. 1. Coordinate systems of a gear pair at the pressure line.

equilibria of the generalized forces for each gear, the coupled equation of motion of a gear pair can be expressed by (a detailed derivation can be found from [3])

$$\left[M^{G'}\right]\left\{\ddot{q}^{G'}\right\} + \left\{\left[C^{G'}\right] + \left[G^{G'}\right]\right\}\left\{\dot{q}^{G'}\right\} + \left[K^{G'}\right]\left\{q^{G'}\right\} = \left\{Q^{G'}\right\}, \tag{2}$$

where $\left[M^{G'}\right]$, $\left[C^{G'}\right]$, $\left[G^{G'}\right]$ and $\left[K^{G'}\right]$ are the inertia, damping, gyroscopic and stiffness matrices and they are given in Appendix A by Eqs. (A.1)–(A.4). It can be noticed that the gear meshing stiffness and damping are coupling mechanisms. And $\left\{Q^{G'}\right\}$ is the external force vector, which is generally a function of gear unbalances, geometrical eccentricities and transmission errors [9]. But the gear meshing damping and the general forces due to gear geometrical eccentricities and transmission errors are not considered in the proceeding analysis. With respect to the global coordinate system as shown in Fig. 2, a generalized displacement vector of a gear pair can be defined by

$$\left\{q^G\right\} = \left\lfloor u_1^G \;\; v_1^G \;\; \theta_{X1}^G \;\; \theta_{Y1}^G \;\; u_2^G \;\; v_2^G \;\; \theta_{X2}^G \;\; \theta_{Y2}^G \;\; \theta_{Z1}^G \;\; \theta_{Z2}^G \right\rfloor^{\mathrm{T}}. \tag{3}$$

Then, through a coordinate transformation considering a pressure angle, the global equation of motion of a gear pair can be expressed by

$$\left[M^G\right]\left\{\ddot{q}^G\right\} + \left\{\left[C^G\right] + \left[G^G\right]\right\}\left\{\dot{q}^G\right\} + \left[K^G\right]\left\{q^G\right\} = \left\{Q^G\right\}. \tag{4}$$

Fig. 3 shows the structure of the global coupled gear mesh stiffness matrix, $\left[K^G\right]$. $k_{l1,2}$ and k_{lc} represent the pure lateral components and the coupled component between the lateral vibrations and $k_{t1,2}$ and k_{tc} the pure torsional components and the coupled component between the torsional

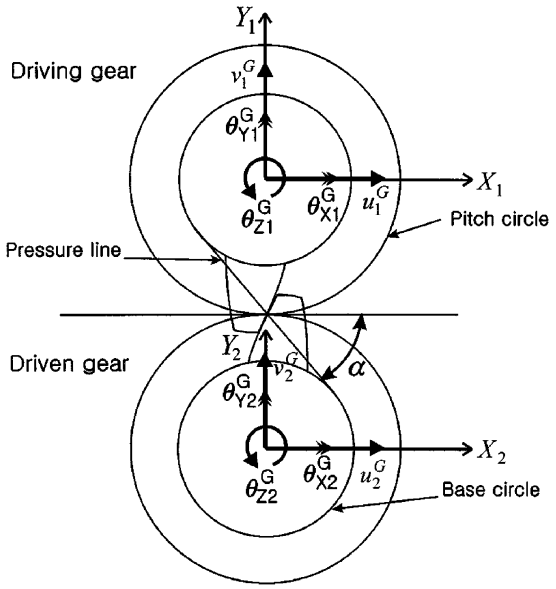

Fig. 2. Global coordinate systems of a gear pair.

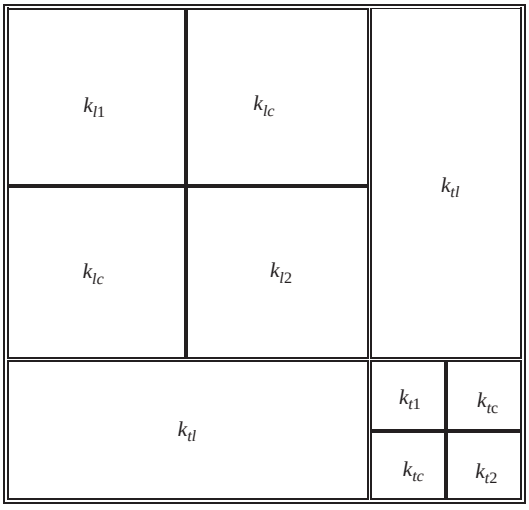

Fig. 3. Structure of a coupled gear mesh stiffness matrix.

vibrations, respectively. And k_{tl} represents the coupled component between the lateral and torsional vibrations.

In order to construct an entire system equation, an assembly of the coupled vibration FE model of a gear pair and the general lateral and torsional vibration FE models of the shafts, bearings and

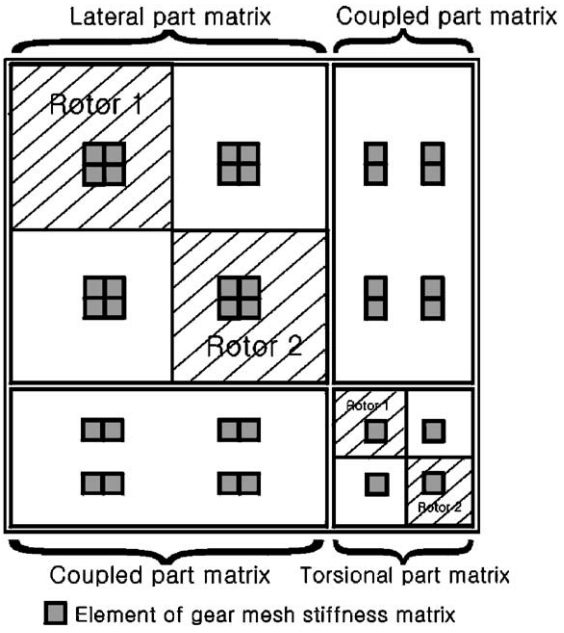

Fig. 4. Structure of an entire assembled stiffness matrix.

disks [16] may be readily implemented by placing the matrices of the pure lateral and torsional vibrations diagonally and the matrices of the coupled vibrations off-diagonally (Refer to Fig. 4, which shows the arrangement of an entire assembled stiffness matrix for instance). Then, the generalized equations of motion of an entire geared two-shaft rotor-bearing system may be given by

$$[M]\{\ddot{q}\} + [C]\{\dot{q}\} + [K]\{q\} = \{Q\}. \tag{5}$$

3. Unbalance response formulation

Considering the driving and driven speeds, ω_1 and ω_2, of the two rotor shafts, the generalized unbalance exciting force, $\{Q\}$, and the unbalance response solution, $\{q\}$, of Eq. (5) are expressed by

$$\{Q\} = \omega_1^2\{U_c\}_1 \cos\,\omega_1 t + \omega_1^2\{U_s\}_1 \sin\,\omega_1 t + \omega_2^2\{U_c\}_2 \cos\,\omega_2 t + \omega_2^2\{U_s\}_2 \sin\,\omega_2 t, \tag{6}$$

$$\{q\} = \{a\} \cos\,\omega_1 t + \{b\} \sin\,\omega_1 t + \{c\} \cos\,\omega_2 t + \{d\} \sin\,\omega_2 t. \tag{7}$$

$\{U_c\}$ and $\{U_s\}$ are the coefficients of the generalized unbalance exciting force, $\{a\}$, $\{b\}$, $\{c\}$, and $\{d\}$ are the coefficients of the unbalance response solution. Substituting Eqs. (6) and (7) into Eq. (5),

the unbalance response matrix equation is given by

$$\begin{bmatrix} [K]-\omega_1^2[M] & \omega_1[C] & 0 & 0 \\ -\omega_1[C] & [K]-\omega_1^2[M] & 0 & 0 \\ 0 & 0 & [K]-\omega_2^2[M] & \omega_2[C] \\ 0 & 0 & -\omega_2[C] & [K]-\omega_2^2[M] \end{bmatrix} \begin{Bmatrix} \{a\} \\ \{b\} \\ \{c\} \\ \{d\} \end{Bmatrix} = \begin{Bmatrix} \omega_1^2\{U_c\}_1 \\ \omega_1^2\{U_s\}_1 \\ \omega_2^2\{U_c\}_2 \\ \omega_2^2\{U_s\}_2 \end{Bmatrix}. \tag{8}$$

From the coefficients of the unbalance response solution obtained from Eq. (8), horizontal and vertical responses, q_1 and q_2, at any station or node are expressed by

$$q_1 = a_1 \cos \omega_1 t + b_1 \sin \omega_1 t + c_1 \cos \omega_2 t + d_1 \sin \omega_2 t, \tag{9}$$

$$q_2 = a_2 \cos \omega_1 t + b_2 \sin \omega_1 t + c_2 \cos \omega_2 t + d_2 \sin \omega_2 t. \tag{10}$$

Then, the radius of the unbalance response orbit shown in Fig. 5 is obtained by utilizing the trigonometric formula

$$\begin{aligned} r &= \sqrt{q_1^2 + q_2^2} \\ &= \left[\tfrac{1}{2}\{(a_1^2 + b_1^2 + c_1^2 + d_1^2 + a_2^2 + b_2^2 + c_2^2 + d_2^2) + (a_1^2 - b_1^2 + a_2^2 - b_2^2)\cos 2\omega_1 t \right. \\ &\quad + (c_1^2 - d_1^2 + c_2^2 - d_2^2)\cos 2\omega_2 t + 2(a_1 b_1 + a_2 b_2)\sin 2\omega_1 t + 2(c_1 d_1 + c_2 d_2)\sin 2\omega_2 t \\ &\quad + 4(a_1 c_1 + a_2 c_2)\cos \omega_1 t \cdot \cos \omega_2 t + 4(b_1 d_1 + b_2 d_2)\sin \omega_1 t \cdot \sin \omega_2 t \\ &\quad \left. +4(a_1 d_1 + a_2 d_2)\cos \omega_1 t \cdot \sin \omega_2 t + 4(b_1 c_1 + b_2 c_2)\sin \omega_1 t \cdot \cos \omega_2 t\}\right]^{1/2}. \end{aligned} \tag{11}$$

Further, the conditions under which r has the maximum and minimum values are obtained from Eqs. (12) and (13) and they are given by Eqs. (14)–(17):

$$\frac{\partial r}{\partial(\omega_1 t)} = 0, \tag{12}$$

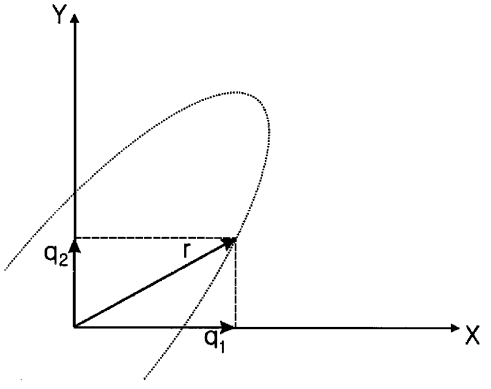

Fig. 5. An orbit of unbalance response.

$$\frac{\partial r}{\partial(\omega_2 t)} = 0, \tag{13}$$

$$-2(a_1^2 - b_1^2 + a_2^2 - b_2^2)\sin 2\omega_1 t + 4(a_1 b_1 + a_2 b_2)\cos 2\omega_1 t = 0, \tag{14}$$

$$\begin{aligned} &-4(a_1 c_1 + a_2 c_2)\sin \omega_1 t \cdot \cos \omega_2 t + 4(b_1 d_1 + b_2 d_2)\cos \omega_1 t \cdot \sin \omega_2 t \\ &-4(a_1 d_1 + a_2 d_2)\sin \omega_1 t \cdot \sin \omega_2 t + 4(b_1 c_1 + b_2 c_2)\cos \omega_1 t \cdot \cos \omega_2 t = 0, \end{aligned} \tag{15}$$

$$-2(c_1^2 - d_1^2 + c_2^2 - d_2^2)\sin 2\omega_2 t + 4(c_1 d_1 + c_2 d_2)\cos 2\omega_2 t = 0, \tag{16}$$

$$\begin{aligned} &-4(a_1 c_1 + a_2 c_2)\cos \omega_1 t \cdot \sin \omega_2 t + 4(b_1 d_1 + b_2 d_2)\sin \omega_1 t \cdot \cos \omega_2 t \\ &+4(a_1 d_1 + a_2 d_2)\cos \omega_1 t \cdot \cos \omega_2 t - 4(b_1 c_1 + b_2 c_2)\sin \omega_1 t \cdot \sin \omega_2 t = 0. \end{aligned} \tag{17}$$

After a lengthy manipulation of Eqs. (14)–(17) utilizing the trigonometric formula, the following final condition equations are resulted:

$$\cos 2\omega_1 t = \pm \frac{(a_1^2 - b_1^2 + a_2^2 - b_2^2)}{\left[(a_1^2 - b_1^2 + a_2^2 - b_2^2)^2 + 4(a_1 b_1 + a_2 b_2)^2\right]^{1/2}}, \tag{18}$$

$$\sin 2\omega_1 t = \pm \frac{2(a_1 b_1 + a_2 b_2)}{\left[(a_1^2 - b_1^2 + a_2^2 - b_2^2)^2 + 4(a_1 b_1 + a_2 b_2)^2\right]^{1/2}}, \tag{19}$$

$$\cos 2\omega_2 t = \pm \frac{(c_1^2 - d_1^2 + c_2^2 - d_2^2)}{\left[(c_1^2 - d_1^2 + c_2^2 - d_2^2)^2 + 4(c_1 d_1 + c_2 d_2)^2\right]^{1/2}}, \tag{20}$$

$$\sin 2\omega_2 t = \pm \frac{2(c_1 d_1 + c_2 d_2)}{\left[(c_1^2 - d_1^2 + c_2^2 - d_2^2)^2 + 4(c_1 d_1 + c_2 d_2)^2\right]^{1/2}}, \tag{21}$$

$$\cos \omega_1 t \cdot \cos \omega_2 t = \pm \frac{1}{2}\left[\frac{\alpha}{\sqrt{\alpha^2 + \beta^2}} \pm \frac{\gamma}{\sqrt{\gamma^2 + \delta^2}}\right], \tag{22}$$

$$\sin \omega_1 t \cdot \sin \omega_2 t = \mp \frac{1}{2}\left[\frac{\alpha}{\sqrt{\alpha^2 + \beta^2}} \mp \frac{\gamma}{\sqrt{\gamma^2 + \delta^2}}\right], \tag{23}$$

$$\sin \omega_1 t \cdot \cos \omega_2 t = \pm \frac{1}{2}\left[\frac{\beta}{\sqrt{\alpha^2+\beta^2}} \pm \frac{\delta}{\sqrt{\gamma^2+\delta^2}}\right], \tag{24}$$

$$\cos \omega_1 t \cdot \sin \omega_2 t = \pm \frac{1}{2}\left[\frac{\beta}{\sqrt{\alpha^2+\beta^2}} \mp \frac{\delta}{\sqrt{\gamma^2+\delta^2}}\right], \tag{25}$$

where α, β, γ, and δ are defined by

$$\begin{aligned}
\alpha &= a_1c_1 - b_1d_1 + a_2c_2 - b_2d_2,\\
\beta &= a_1d_1 + b_1c_1 + a_2d_2 + b_2c_2,\\
\gamma &= a_1c_1 + b_1d_1 + a_2c_2 + b_2d_2,\\
\delta &= b_1c_1 - a_1d_1 + b_2c_2 - a_2d_2.
\end{aligned}$$

Finally, substituting Eqs. (18)–(25) into Eq. (11) and comparing the corresponding values of r for each combination of these condition equations, the maximum and minimum radii of the unbalance response orbit are given by

$$\begin{aligned}
r_{\substack{\max\\ \min}} = \frac{1}{\sqrt{2}}\Bigg\{ & (a_1^2+b_1^2+c_1^2+d_1^2+a_2^2+b_2^2+c_2^2+d_2^2)\\
& \pm [(a_1^2-b_1^2+a_2^2-b_2^2)^2 + 4(a_1b_1+a_2b_2)^2]^{1/2}\\
& \pm [(c_1^2-d_1^2+c_2^2-d_2^2)^2 + 4(c_1d_1+c_2d_2)^2]^{1/2}\\
& \pm 2(a_1c_1+a_2c_2)\left[\frac{\alpha}{\sqrt{\alpha^2+\beta^2}} + \frac{\gamma}{\sqrt{\gamma^2+\delta^2}}\right]\\
& \mp 2(b_1d_1+b_2d_2)\left[\frac{\alpha}{\sqrt{\alpha^2+\beta^2}} - \frac{\gamma}{\sqrt{\gamma^2+\delta^2}}\right]\\
& \pm 2(a_1d_1+a_2d_2)\left[\frac{\beta}{\sqrt{\alpha^2+\beta^2}} - \frac{\delta}{\sqrt{\gamma^2+\delta^2}}\right]\\
& \pm 2(b_1c_1+b_2c_2)\left[\frac{\beta}{\sqrt{\alpha^2+\beta^2}} + \frac{\delta}{\sqrt{\gamma^2+\delta^2}}\right]\Bigg\}^{1/2}.
\end{aligned} \tag{26}$$

4. Analysis results and discussions

Applying the proposed method, an unbalance response analysis has been performed with a 600 kW turbo-chiller rotor-bearing system shown in Fig. 6, having a bull-pinion speed increasing gear. The driver rotor-bearing system consists of the motor and bull gear with a rated speed of 3420 rev/min. And the driven rotor-bearing system consists of the compressor impeller and pinion gear with a rated speed of 11,845 rev/min. The FE modeling data of the turbo-chiller

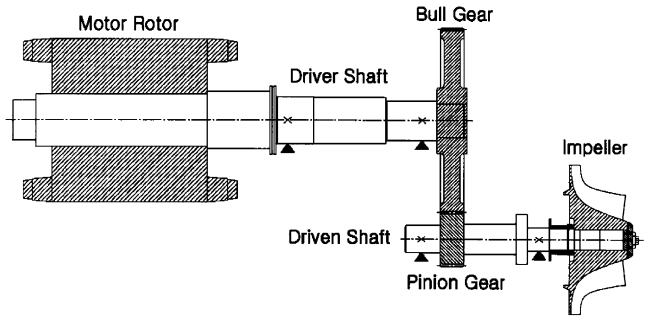

Fig. 6. Schematic of a 600 kW turbo-chiller rotor-bearing system.

Table 1
Driver and driven shaft element data for the FE model

Driver shaft element (mm)				Driven shaft element (mm)			
Length		Diameter		Length		Diameter	
1	50	1	84	1	34.3	1	57
2	35	2	110	2	40	2	57
3	110	3	110	3	25	3	110.9
4	110	4	110	4	25	4	110.9
5	110	5	110	5	37	5	63.5
6	44	6	120	6	37.6	6	63.5
7	45	7	120	7	37	7	63.5
8	44	8	120	8	23.4	8	104
9	13	9	142.8	9	25.2	9	48
10	25	10	98	10	21.3	10	48
11	55	11	98	11	20.1	11	44
12	50	12	96	12	20.1	12	44
13	55	13	96	13	13.9	13	44
14	50	14	96	14	28.4	14	44
15	38	15	84	15	27.2	15	44
16	39	16	84		$\rho = 7833\,\mathrm{kg/m^3}$		
17	31.6	17	84		$E = 200\mathrm{E}9\,\mathrm{Pa}$		
18	33	18	70		$G = 793\mathrm{E}8\,\mathrm{Pa}$		
19	25	19	70				

Table 2
Lumped inertias and bearing coefficients for the FE model

Driver rotor				Driven rotor			
	M (kg)	I_p (kg m^2)	I_t (kg m^2)		M (kg)	I_p (kg m^2)	I_t (kg m^2)
D1	35.10	0.56	0.32	D5	0.52	4.31E–4	3.04E–4
D2	70.19	1.12	0.63	D6	0.14	1.08E–4	6.04E–5
D3	70.19	1.12	0.63	D7	5.75	3.56E–2	2.39E–2
D4	35.10	0.56	0.32	D8	0.40	2.21E–4	2.06E–3
G1	35.04	0.66	0.34				

Bearing stiffness and damping at 3420 (rev/min)

	K_{XX} (N/m)	K_{XY} (N/m)	K_{YX} (N/m)	K_{YY} (N/m)	D_{XX} (N s/m)	D_{XY} (N s/m)	D_{YX} (N s/m)	D_{YY} (N s/m)
B1	0.187E9	0.751E8	−0.198E9	0.708E8	0.877E6	−0.462E6	−0.462E6	0.703E6
B2	0.601E9	0.510E9	−0.220E9	0.175E9	0.339E7	−0.230E5	−0.228E5	0.934E6
B3	0.860E8	0.284E9	−0.105E9	0.247E9	0.337E6	0.219E6	0.219E6	0.347E6
B4	0.774E8	0.220E9	−0.295E8	0.131E9	0.292E6	0.142E6	0.142E6	0.134E6

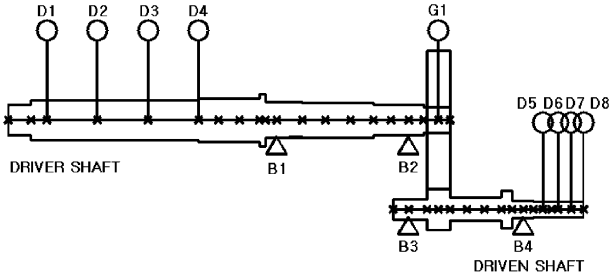

Fig. 7. An equivalent FE model of the turbo-chiller rotor-bearing system.

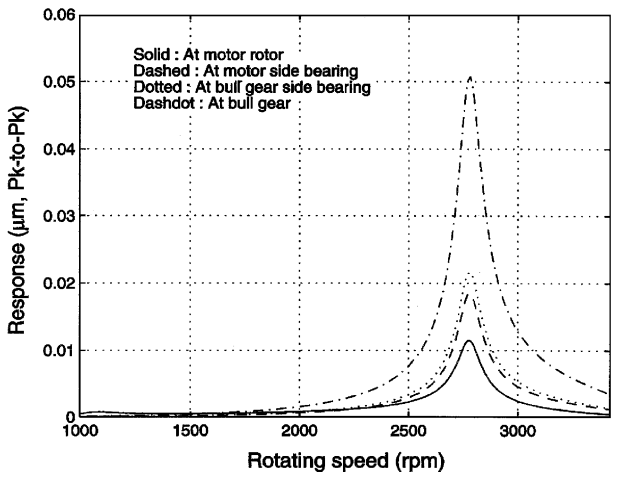

Fig. 8. Coupled unbalance responses for the driver rotor system with a test unbalance attached to the compressor impeller.

rotor-bearing system and its equivalent FE model are given in Tables 1 and 2 and in Fig. 7. In the analysis the rotating speed-dependent dynamic coefficients of support journal bearings were used.

As analyzed with test unbalances of U_{M1} (2018.5 g mm) and U_{M2} (873.0 g mm), attached 180° out-of-phase to the motor rotor and bull gear, the maximum (peak-to-peak) coupled unbalance responses at the motor rotor and impeller were less than 60 and 0.06 μm each. As analyzed with a test unbalance of U_I (19.7 g mm) attached to the impeller, the maximum coupled unbalance responses at the motor rotor and impeller were less than 0.06 and 6 μm each. Therefore, the unbalance lateral-coupling effects between the two rotor systems are very limited. But

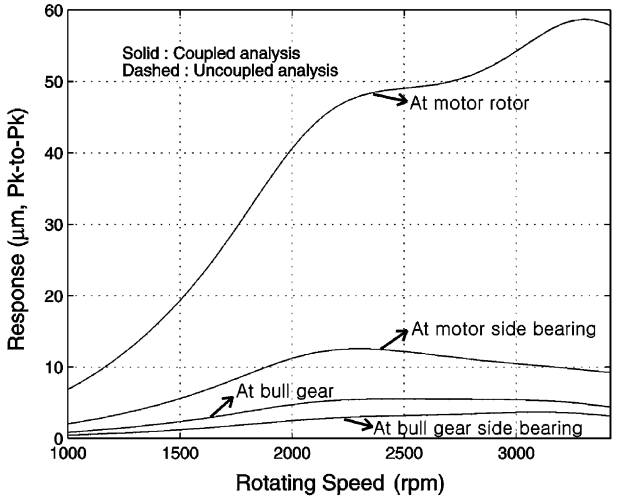

Fig. 9. Coupled and uncoupled unbalance responses for the driver rotor system with a full set of test unbalances.

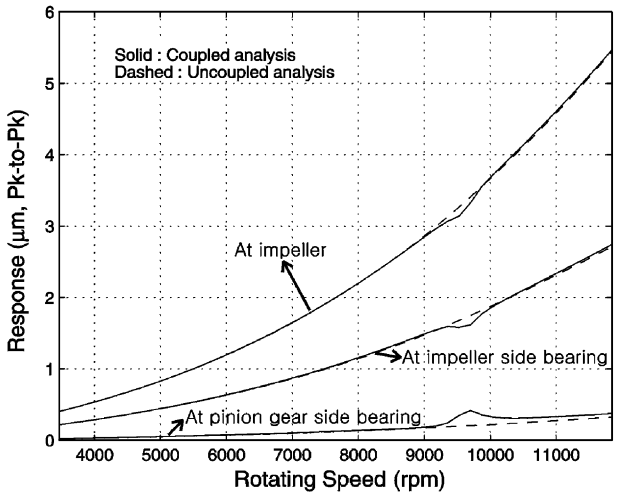

Fig. 10. Coupled and uncoupled unbalance responses for the driven rotor system with a full set of test unbalances.

amplifications of the responses at the driver rotor system with U_I attached to the impeller were observed as shown in Fig. 8 at 2778 rev/min, which corresponds to a driven rotor speed of 9621 rev/min. This speed exactly coincides with the first torsional natural frequency of the system (refer [3]). Thus, it is reasonable to assume that the torsional resonance has influenced the lateral unbalance responses because of the coupling effect of the lateral and torsional dynamics due to gear meshing.

As analyzed with test unbalances of U_{M1} and U_{M2} attached to the motor rotor and bull gear, respectively and U_I attached to the impeller (with 180°out-of-phase between U_{M1} and U_{M2}, and in-phase between U_{M1} and U_I), the maximum coupled and uncoupled unbalance response results are shown in Figs. 9 and 10. Fig. 9 shows that at the driver rotor system no difference of

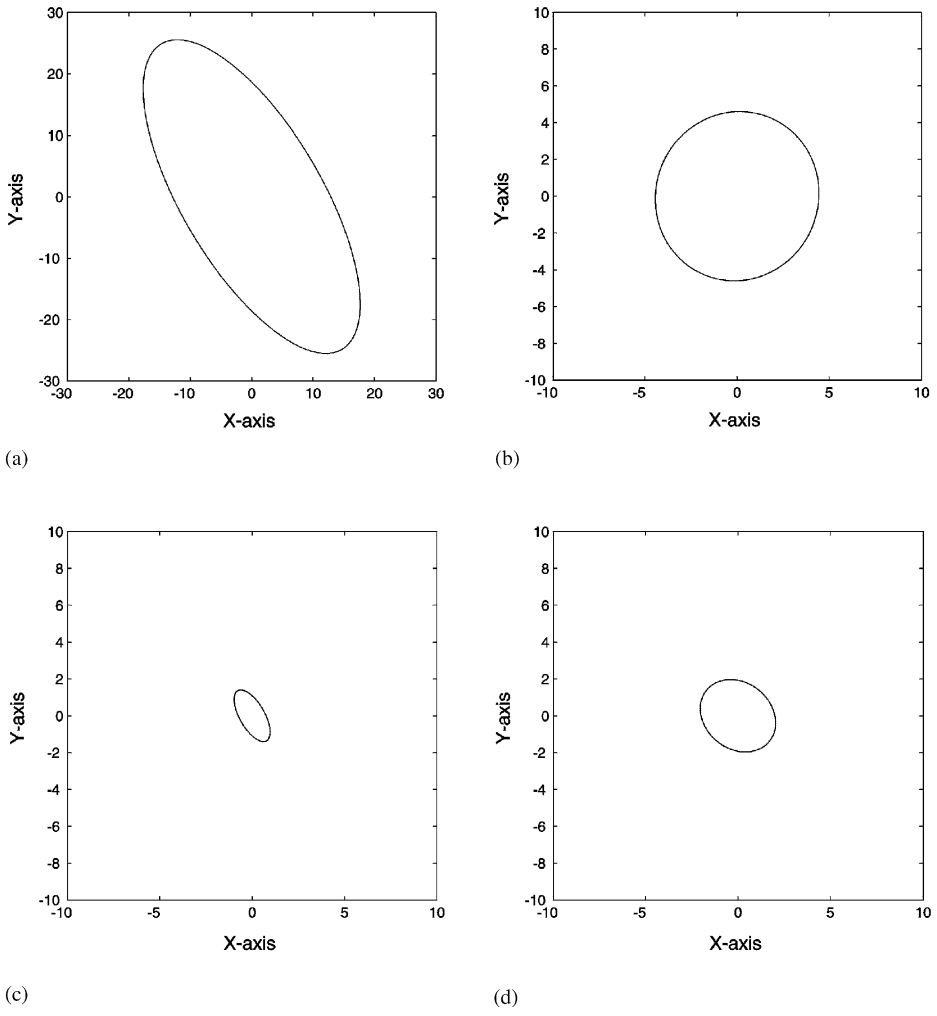

Fig. 11. Coupled unbalance response orbits for the driver rotor system at a driver speed of 3,420 rev/min with a full set of test unbalances. (a) At motor rotor, (b) at motor side bearing, (c) at bull gear side bearing, (d) at bull gear.

unbalance responses between the coupled and uncoupled analyses is evident. At the driven rotor system it can be observed in Fig. 10 that the coupled and uncoupled unbalance responses are almost identical, except that the coupled responses have some bumps at 9621 rev/min due to the torsional resonance, again. Further, the unbalance response orbits calculated at a driver speed of 3420 rev/min are shown in Figs. 11 and 12 for various locations of the driver and driven rotor systems. Since the orbit components of one rotor speed are dominant, as shown in Figs. 11 and 12 except for the orbit at the pinion side bearing position (Fig. 12(a)), the lateral coupling between the two rotor systems can, again, be confirmed as very limited. However, at the pinion side bearing position the unbalance response due to U_I, attached to the impeller, happened to be quite

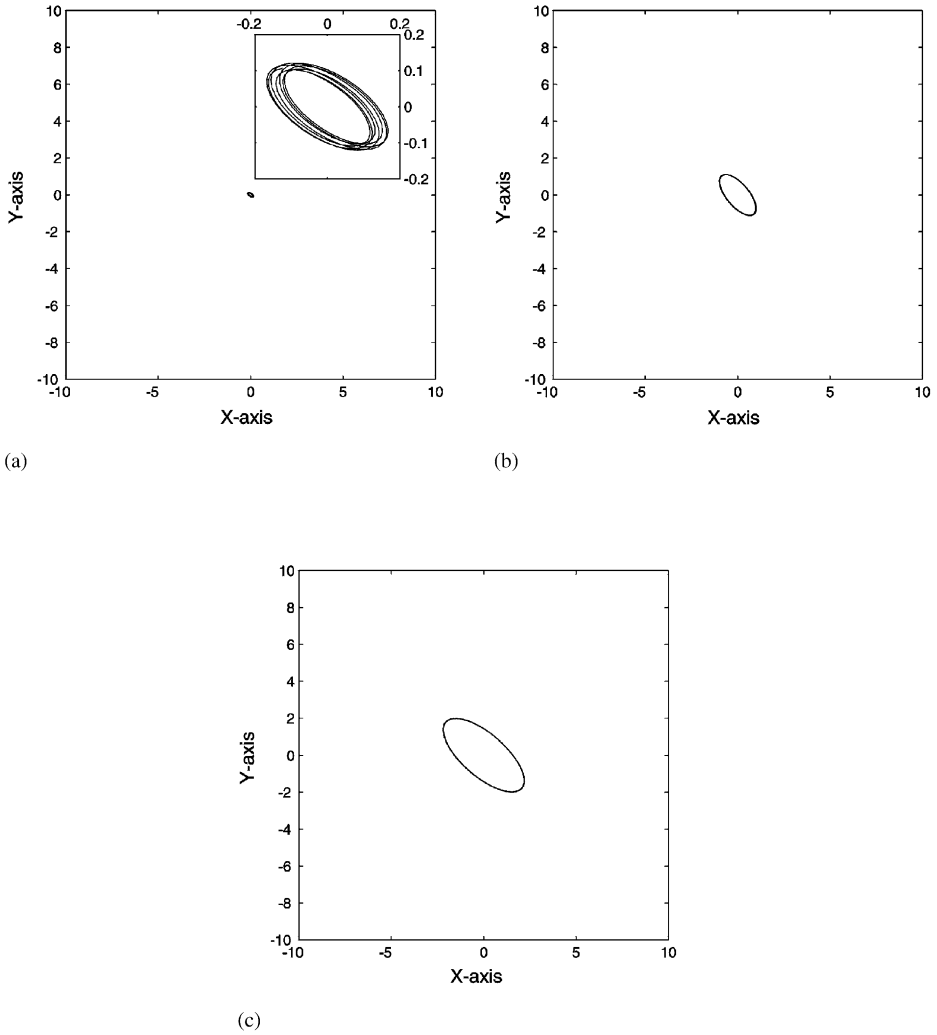

Fig. 12. Coupled unbalance response orbits for the driven rotor system at a driver speed of 3,420 rev/min with a full set of test unbalances. (a) At pinion gear side bearing, (b) at impeller side bearing (c) at impeller.

Table 3
Errors of the maximum coupled unbalance responses as obtained by the proposed closed-form solution and full numerical approach at a driver speed of 3420 rev/min with a full set of test unbalances

Location	Errors (percent) of response		
	Sample number per revolution		
	10	100	1000
Motor rotor	0.8784	0.0152	0.0005
Motor side bearing	0.2139	0.0086	0.0043
Bull gear side bearing	0.1660	0.0128	0.0128
Bull gear	0.3800	0.0660	0.0637
Pinion side bearing	0.4000	0.4000	0.4000
Impeller side bearing	0.7805	0.1568	0.1568
Impeller	0.3601	0.2486	0.0329

small enough that the coupled unbalance effects from U_{M1} and U_{M2} were able to appear in the Fig. 12(a).

For a validation of the proposed analytical solutions of the orbit radii, Table 3 shows the errors (percent) of the maximum coupled unbalance responses as obtained by the proposed closed-form solution and full numerical approach at a driver speed of 3420 rev/min. The entity in the table "sample number per revolution" represents the number of sample data per revolution used to determine the maximum responses by the full numerical approach. As the sample number increases to over 100, the errors between them decrease further to a great extent except for the responses at the pinion side bearing position where the orbit components of two rotor speeds are more pronounced, as shown in Fig. 12(a). In addition, Figs. 13 and 14 show the maximum coupled unbalance responses for the driver and driven rotor systems, respectively, with a full set of test unbalances as obtained by the proposed and full numerical methods using 10 samples. It can be seen that the responses by the two methods agree well for the range of operating speeds.

5. Conclusions

In this paper a general method had been presented for obtaining the unbalance response orbit of a gear-coupled two-shaft rotor-bearing system, based on the finite element approach. Specifically, analytical solutions of the maximum and minimum radii of the orbit had been proposed. The method was applied to the unbalance response analysis of a 600 kW turbo-chiller rotor-bearing system, having a bull-pinion speed increasing gear. Bumps in the unbalance responses for the high-speed compressor rotor system were observed at the first torsional natural frequency by the coupling effect between the lateral and torsional dynamics due to gear meshing. However, it was predicted that the lateral coupling between the driver and driven rotor systems is very limited. Further, the proposed analytical solutions were validated with those obtained by a

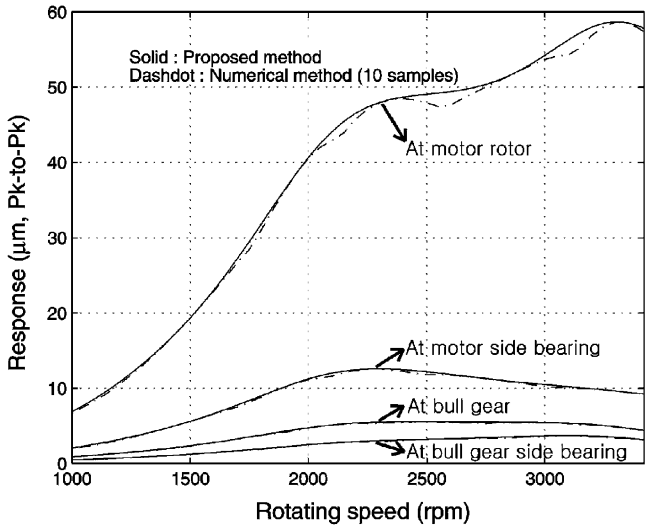

Fig. 13. Coupled unbalance responses for the driver rotor system with a full set of test unbalances as obtained by the proposed and full numerical methods using 10 samples.

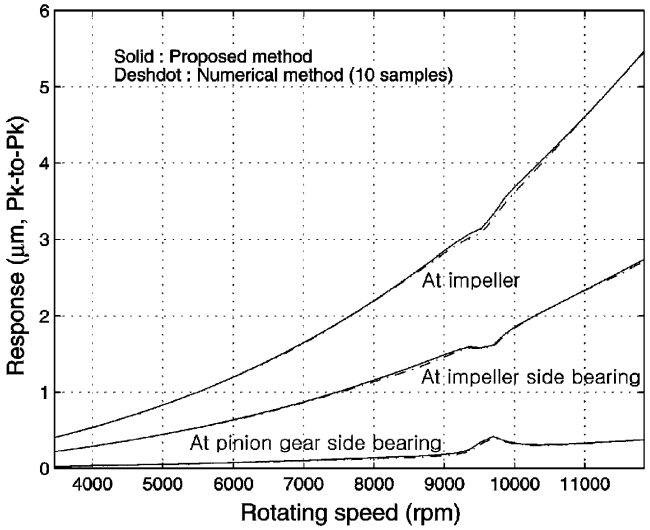

Fig. 14. Coupled unbalance responses for the driven rotor system with a full set of test unbalances as obtained by the proposed and full numerical methods using 10 samples.

full numerical approach. The proposed method can be generally applied to the analysis of the unbalance response orbits of dual-shaft rotor-bearing systems coupled by bearings as well, which are often found in aerospace gas turbine engines.

Appendix A

$$\left[M^{G'}\right] = \begin{bmatrix} M_1^G & 0 & 0 & 0 & 0 & 0 & 0 & 0 & 0 & 0 \\ 0 & M_1^G & 0 & 0 & 0 & 0 & 0 & 0 & 0 & 0 \\ 0 & 0 & I_{t1}^G & 0 & 0 & 0 & 0 & 0 & 0 & 0 \\ 0 & 0 & 0 & I_{t1}^G & 0 & 0 & 0 & 0 & 0 & 0 \\ 0 & 0 & 0 & 0 & M_2^G & 0 & 0 & 0 & 0 & 0 \\ 0 & 0 & 0 & 0 & 0 & M_2^G & 0 & 0 & 0 & 0 \\ 0 & 0 & 0 & 0 & 0 & 0 & I_{t2}^G & 0 & 0 & 0 \\ 0 & 0 & 0 & 0 & 0 & 0 & 0 & I_{t2}^G & 0 & 0 \\ 0 & 0 & 0 & 0 & 0 & 0 & 0 & 0 & I_{p1}^G & 0 \\ 0 & 0 & 0 & 0 & 0 & 0 & 0 & 0 & 0 & I_{p2}^G \end{bmatrix}, \tag{A.1}$$

$$\left[C^{G'}\right] = c_m \begin{bmatrix} 0 & 0 & 0 & 0 & 0 & 0 & 0 & 0 & 0 & 0 \\ 0 & 1 & 0 & 0 & 0 & -1 & 0 & 0 & r_1 & r_2 \\ 0 & 0 & 0 & 0 & 0 & 0 & 0 & 0 & 0 & 0 \\ 0 & 0 & 0 & 0 & 0 & 0 & 0 & 0 & 0 & 0 \\ 0 & 0 & 0 & 0 & 0 & 0 & 0 & 0 & 0 & 0 \\ 0 & -1 & 0 & 0 & 0 & 1 & 0 & 0 & -r_1 & -r_2 \\ 0 & 0 & 0 & 0 & 0 & 0 & 0 & 0 & 0 & 0 \\ 0 & 0 & 0 & 0 & 0 & 0 & 0 & 0 & 0 & 0 \\ 0 & r_1 & 0 & 0 & 0 & -r_1 & 0 & 0 & r_1^2 & r_1 r_2 \\ 0 & r_2 & 0 & 0 & 0 & -r_2 & 0 & 0 & r_1 r_2 & r_2^2 \end{bmatrix}, \tag{A.2}$$

$$\left[G^{G'}\right] = \begin{bmatrix} 0 & 0 & 0 & 0 & 0 & 0 & 0 & 0 & 0 & 0 \\ 0 & 0 & 0 & 0 & 0 & 0 & 0 & 0 & 0 & 0 \\ 0 & 0 & 0 & I_{p1}^G \Omega_1 & 0 & 0 & 0 & 0 & 0 & 0 \\ 0 & 0 & -I_{p1}^G \Omega_1 & 0 & 0 & 0 & 0 & 0 & 0 & 0 \\ 0 & 0 & 0 & 0 & 0 & 0 & 0 & 0 & 0 & 0 \\ 0 & 0 & 0 & 0 & 0 & 0 & 0 & 0 & 0 & 0 \\ 0 & 0 & 0 & 0 & 0 & 0 & 0 & I_{p2}^G \Omega_2 & 0 & 0 \\ 0 & 0 & 0 & 0 & 0 & 0 & -I_{p2}^G \Omega_2 & 0 & 0 & 0 \\ 0 & 0 & 0 & 0 & 0 & 0 & 0 & 0 & 0 & 0 \\ 0 & 0 & 0 & 0 & 0 & 0 & 0 & 0 & 0 & 0 \end{bmatrix}, \tag{A.3}$$

$$\left[K^{G'}\right] = k_m \begin{bmatrix} 0 & 0 & 0 & 0 & 0 & 0 & 0 & 0 & 0 & 0 \\ 0 & 1 & 0 & 0 & 0 & -1 & 0 & 0 & r_1 & r_2 \\ 0 & 0 & 0 & 0 & 0 & 0 & 0 & 0 & 0 & 0 \\ 0 & 0 & 0 & 0 & 0 & 0 & 0 & 0 & 0 & 0 \\ 0 & 0 & 0 & 0 & 0 & 0 & 0 & 0 & 0 & 0 \\ 0 & -1 & 0 & 0 & 0 & 1 & 0 & 0 & -r_1 & -r_2 \\ 0 & 0 & 0 & 0 & 0 & 0 & 0 & 0 & 0 & 0 \\ 0 & 0 & 0 & 0 & 0 & 0 & 0 & 0 & 0 & 0 \\ 0 & r_1 & 0 & 0 & 0 & -r_1 & 0 & 0 & r_1^2 & r_1 r_2 \\ 0 & r_2 & 0 & 0 & 0 & -r_2 & 0 & 0 & r_1 r_2 & r_2^2 \end{bmatrix}, \tag{A.4}$$

where c_m and k_m are the gear mesh damping and stiffness.

References

[1] R.L. Eshleman, R.A. Eubanks, On the critical speeds of a continuous rotor, *Journal of Engineering for Industry* (1969) 1180–1188.

[2] L.D. Mitchell, D.M. Mellen, Torsional–lateral coupling in a geared high-speed rotor system, ASME Paper 75-DET-75 (1975).

[3] A.S. Lee, J.W. Ha, D.-H. Choi, Coupled lateral and torsional vibration characteristics of a speed increasing geared rotor-bearing system, *Journal of Sound and Vibration* 263 (4) (2003) 725–742.

[4] J.S. Rao, J.R. Chang, T.N. Shiau, Coupled bending–torsion vibration of geared rotors, *ASME DE-Vol. 84-2, Design Engineering Technical Conferences 3 (Part B)* (1995) 977–989.

[5] S.V. Neriya, R.B. Bhat, T.S. Sankar, Coupled torsional flexural vibration of a geared shaft system using finite element method, *The Shock and Vibration Bulletin (Part 3)* 55 (1985) 13–25.

[6] A. Kahraman, H.N. Ozguven, D.R. Houser, J.J. Zakrajsek, Dynamic analysis of geared rotors by finite elements, *Transactions Journal of Mechanical Design* 114 (1992) 507–514.

[7] H. Iida, A. Tamura, K. Kikuch, H. Agata, Coupled torsional-flexural vibration of a shaft in a geared system of rotors (1st report), *Bulletin of the JSME* 23 (186) (1980) 2111–2117.

[8] T. Iwatsubo, S. Arii, R. Kawai, Coupled lateral–torsional vibration of rotor system trained by gears, *Bulletin of JSME* 27 (224) (1984) 271–277.

[9] S.T. Choi, S.Y. Mau, Dynamic analysis of geared rotor-bearing systems by the transfer matrix method, *ASME DE-Vol. 84-2, Design Engineering Technical Conferences 3 (Part B)* (1995) 967–976.

[10] D.H. Hibner, Dynamic response of viscous-damped multi-shaft jet engines, *Journal of Aircraft* 12 (4) (1975) 305–312.

[11] Q. Li, L. Yan, J.F. Hamilton, Investigation of the steady-state response of a dual-rotor system with intershaft squeeze film damper, *Transactions Journal of Engineering for Gas Turbines and Power* 108 (1986) 605–612.

[12] K. Gupta, K.D. Gupta, K. Athre, Unbalance response of a dual rotor system: theory and experiment, *Transactions Journal of Vibration and Acoustics* 115 (1993) 427–435.

[13] J.S. Rao, *Rotor Dynamics*, 3rd ed., New Age International Publishers, 1996.

[14] J.S. Rao, T.N. Shiau, J.R. Chang, Theoretical analysis of lateral response due to torsional excitation of geared rotor, *Mechanism and Machine Theory* 33 (6) (1998) 761–783.

[15] T.N. Shiau, J.S. Rao, J.R. Chang, S.-T. Choi, Dynamic behavior of geared rotors, *Transactions Journal of Engineering for Gas Turbine and Power* 121 (1999) 494–503.

[16] A.S. Lee, Y.S. Lee, Rotordynamic characteristics of an APU gas turbine rotor-bearing system having a tie shaft, *KSME International Journal* 15 (2) (2001) 152–159.